



# CHORUS

This is the accepted manuscript made available via CHORUS. The article has been published as:

Neutron transfer studies on  $^{25}\text{Mg}$  and its correlation to neutron radiative capture processes

Y. Chen, G. P. A. Berg, R. J. deBoer, J. Görres, H. Jung, A. Long, K. Seetedohnia, R. Talwar, M. Wiescher, S. Adachi, H. Fujita, Y. Fujita, K. Hatanaka, C. Iwamoto, B. Liu, S. Noji, H.-J. Ong, and A. Tamii

Phys. Rev. C **103**, 035809 — Published 15 March 2021

DOI: [10.1103/PhysRevC.103.035809](https://doi.org/10.1103/PhysRevC.103.035809)

# Neutron transfer studies on $^{25}\text{Mg}$ and its correlation to neutron radiative capture processes

Y. Chen, G.P.A. Berg, R.J. deBoer, J. Görres, H. Jung,  
A. Long, K. Seetedohnia, R. Talwar, and M. Wiescher  
*The Joint Institute for Nuclear Astrophysics,  
Department of Physics, Notre Dame, Indiana 46556, USA*

S. Adachi, H. Fujita, Y. Fujita, K. Hatanaka, C.  
Iwamoto,\* B. Liu, S. Noji,<sup>†</sup> H.-J. Ong,<sup>‡</sup> and A. Tamii  
*Research Center for Nuclear Physics,  
Osaka University, Ibaraki,  
Osaka 567-0047, Japan*

## Abstract

Radiative neutron capture reactions play an important role in nuclear astrophysics. In some cases direct neutron capture reaction studies are not possible and neutron transfer reactions have been suggested as a surrogate approach. We have performed a detailed study of the  $^{25}\text{Mg}(d,p)^{26}\text{Mg}$  reaction at a beam energy of 56 MeV as a surrogate reaction to the radiative neutron capture reaction  $^{25}\text{Mg}(n,\gamma)^{26}\text{Mg}$ . A large number of neutron bound and unbound states between 10.6 and 12.1 MeV excitation energy in  $^{26}\text{Mg}$  were observed. Angular distribution analysis provided information about the orbital momentum transfer populating these levels. The comparison with resonances observed in the  $^{25}\text{Mg}(n,\gamma)^{26}\text{Mg}$  reaction indicate that different levels in  $^{26}\text{Mg}$  are being populated through the two reaction mechanisms, causing substantial discrepancies in the reaction rate prediction. This result demonstrates that neutron transfer reaction studies may not necessarily lead to reliable predictions for neutron capture reaction rates.

---

\* RIKEN Center for Advanced Photonics (RAP)

<sup>†</sup> NSCL, Michigan State University

<sup>‡</sup> Institute of Modern Physics, Chinese Academy of Sciences

## I. INTRODUCTION

Radiative neutron capture reactions play an important role in nuclear astrophysics as well as in other disciplines ranging from reactor physics to geophysics. In nuclear astrophysics, neutron capture reactions drive the production of heavy elements beyond iron, through the  $s$ -process, along the line of stability [1]. In reactor physics, the question of neutron capture reactions on fission products is important for determining and simulating the efficiency of fuel elements [2]. In geophysics, the  $\alpha$ -particles emitted by the natural decay chains produce a neutron flux through subsequent  $(\alpha, n)$  reactions, which cause secondary radiative neutron captures in the surrounding rock material. This, in turn, can be utilized for elemental analysis purposes [3]. In any of these cases, it is of great importance to know the cross sections of radiative neutron capture reactions. While in general one can argue that the radiative capture follows the  $1/v$  law, driven by  $s$ -wave neutron capture components, resonant contributions and  $p$ -wave non-resonant contributions can significantly modify the neutron capture reaction at higher neutron energies. Sub-threshold states may also modify the  $1/v$  energy dependence of the cross section in the astrophysical energy range of interest.

Neutron capture is sometimes difficult to measure and often, for example in the case of radioactive materials, nearly impossible and requires major new developmental work [4]. For these cases, the study of surrogate reactions has been proposed to indirectly obtain the necessary information [5]. One of the most frequently suggested reactions is the  $(d, p)$  neutron transfer process [6]. The strength of the neutron transfer is reflected in the neutron spectroscopic factor ( $S_n$ ) or alternatively in the asymptotic normalization coefficient (ANC) [7] for bound states. In the case of a final bound state in  $(d, p)$  transfer, these parameters correspond directly to the strength of the non-resonant direct capture to that state in the  $(n, \gamma)$  radiative capture. In the case of a  $(d, p)$  transition to an unbound state, they are correlated with the corresponding resonance strengths ( $\omega\gamma$ ) of the  $(n, \gamma)$  radiative capture process.

An important case is the neutron capture reaction  $^{25}\text{Mg}(n, \gamma)^{26}\text{Mg}$ . It is not only a potential neutron poison in the  $s$ -process, but it also provides information on the strength of the neutron channel for the  $^{22}\text{Ne}(\alpha, n)^{25}\text{Mg}$  reaction, which is considered to be one of the main neutron sources for the  $s$ -process. This reaction has a negative  $Q$ -value of 478.3 keV [8, 9]. The lowest observed resonance is at 703 keV center of mass  $\alpha$ -energy. A long discussed possibility is the contribution of further resonances at lower energies, just above the neutron

threshold [10–12]. A number of indirect studies have been performed to identify possible contributions in the energy range above the neutron threshold at an excitation energy of 11.093 MeV in  $^{26}\text{Mg}$  to identify possible natural parity levels that may contribute to the  $^{22}\text{Ne}(\alpha, n)^{25}\text{Mg}$  reaction. A large number of additional new states have been identified, but their specific association with resonances in the  $^{22}\text{Ne}(\alpha, n)^{25}\text{Mg}$  reaction remains inconclusive [13, 14].

## II. THE CASE OF THE $^{25}\text{Mg}(n, \gamma)^{26}\text{Mg}$ REACTION

A particularly interesting experiment probing the neutron strength distribution in  $^{26}\text{Mg}$  was performed at the n\_TOF spallation facility at CERN. The goal of the study was to provide new information about the resonance structure of the  $^{25}\text{Mg}(n, \gamma)^{26}\text{Mg}$  reaction and, therefore, about neutron unbound states in  $^{26}\text{Mg}$ . These states might also be populated strongly in the  $^{22}\text{Ne}(\alpha, n)^{25}\text{Mg}$  reaction [15, 16], if they have sufficiently large  $\alpha$ -particle widths ( $\Gamma_\alpha$ ). The study identified fifteen low-energy resonances corresponding to excited states in  $^{26}\text{Mg}$  between the neutron threshold at 11.093 MeV and 11.344 MeV excitation energy. The spin and parity of many of these states were extracted from resonance shape analysis using the SAMMY  $R$ -matrix code [17]. While, for five states, no spin values could be determined, five other states received an unnatural parity assignment, and five more had natural parity. The observed resonances correspond very well to the unbound levels investigated in non-selective  $^{26}\text{Mg}(p, p)$  and  $^{26}\text{Mg}(d, d)$  inelastic scattering experiments [13].

The goal of this work is to investigate if the  $^{25}\text{Mg}(n, \gamma)^{26}\text{Mg}$  radiative neutron capture data can be mimicked by the  $(d, p)$  surrogate neutron transfer reaction as argued above. This is a case where, up to  $\approx 500$  keV above the neutron threshold, the cross section seems to be determined by narrow, well-separated resonances. The strength of  $(d, p)$  transitions gives the  $S$  or ANC for the neutron transfer. This corresponds to the neutron partial width ( $\Gamma_n$ ) of the resonance states. For transitions to neutron bound states these values would be directly proportional to the cross section  $\sigma$  of the non-resonant direct capture component of the reaction. As such, they provide important insight, in particular for the capture of  $s$ -wave ( $\ell = 0$ ) neutrons with a cross section increasing towards low energies following the  $1/v$  law. At higher energies, contributions of neutron capture at higher orbital momentum  $\ell$  can be anticipated. However, in particular, for neutron capture on heavy nuclei with high level

density at higher excitation energies, these direct capture transitions may be dominated by the low-energy tails of broad, high-energy  $s$ -wave resonances or also by the high-energy tails of sub-threshold states.

For neutron unbound states,  $S$  can be converted into  $\Gamma_n$  with the aid of a nuclear reaction model like the Distorted Wave Born Approximation (DWBA). These calculations will be described in detail in section IV. This approach has been very successful for the determination of resonance strengths in proton capture reactions. The strength of a  $(d, n)$  or  $(d, p)$  reaction yields the  $S$  for the unbound state, and the partial width is given by

$$\Gamma \sim S \cdot \Gamma_{sp}, \quad (1)$$

where  $\Gamma_{sp}$  is the single-particle width determined from theory.

For low-energy resonances of importance for proton-induced nucleosynthesis such as in the CNO cycles and the  $rp$ -process [18], the proton width ( $\Gamma_p$ ) is reduced by the penetrability ( $P_\ell$ ) through Coulomb and orbital momentum barriers. The  $\Gamma_p$  is therefore much smaller than the  $\gamma$ -width ( $\Gamma_\gamma$ ) and the latter determines the total width of the level unless other reaction channels are open. A typical  $\omega\gamma$  [19] in a radiative proton capture reaction is therefore directly proportional to  $\Gamma_p$ , which can be determined in a transfer experiment

$$\omega\gamma = \omega \frac{\Gamma_p \cdot \Gamma_\gamma}{\Gamma_p + \Gamma_\gamma} \approx \omega\Gamma_p. \quad (2)$$

The factor  $\omega$  depends on the spin of the target nucleus, projectile and resonance state. This is a powerful indirect approach for determining resonance strengths in radiative proton or also  $\alpha$ -capture reactions because the Coulomb barrier reduces the charged particle widths to values far below of the typical range of the  $\Gamma_\gamma$ . For radiative neutron capture reactions, the situation is different because of the lack of the Coulomb barrier. The  $\Gamma_n$  is expected to be significantly larger than  $\Gamma_\gamma$ , unless the level has a very small single-particle component or a higher orbital momentum with  $\ell > 0$ . The capture cross section would then be subject to the orbital momentum barrier. Fig. 1 shows the penetrability for neutrons of different orbital momenta as a function of neutron energy. The figure demonstrates that the orbital momentum barrier only causes a significant reduction of the penetrability and the  $\Gamma_n$  for very low energies and high  $\ell$  values.

In cases of resonances populated by low  $\ell$  neutrons, the resonance strength of radiative neutron capture is strongly influenced by  $\Gamma_\gamma$ , which is often significantly smaller or at least

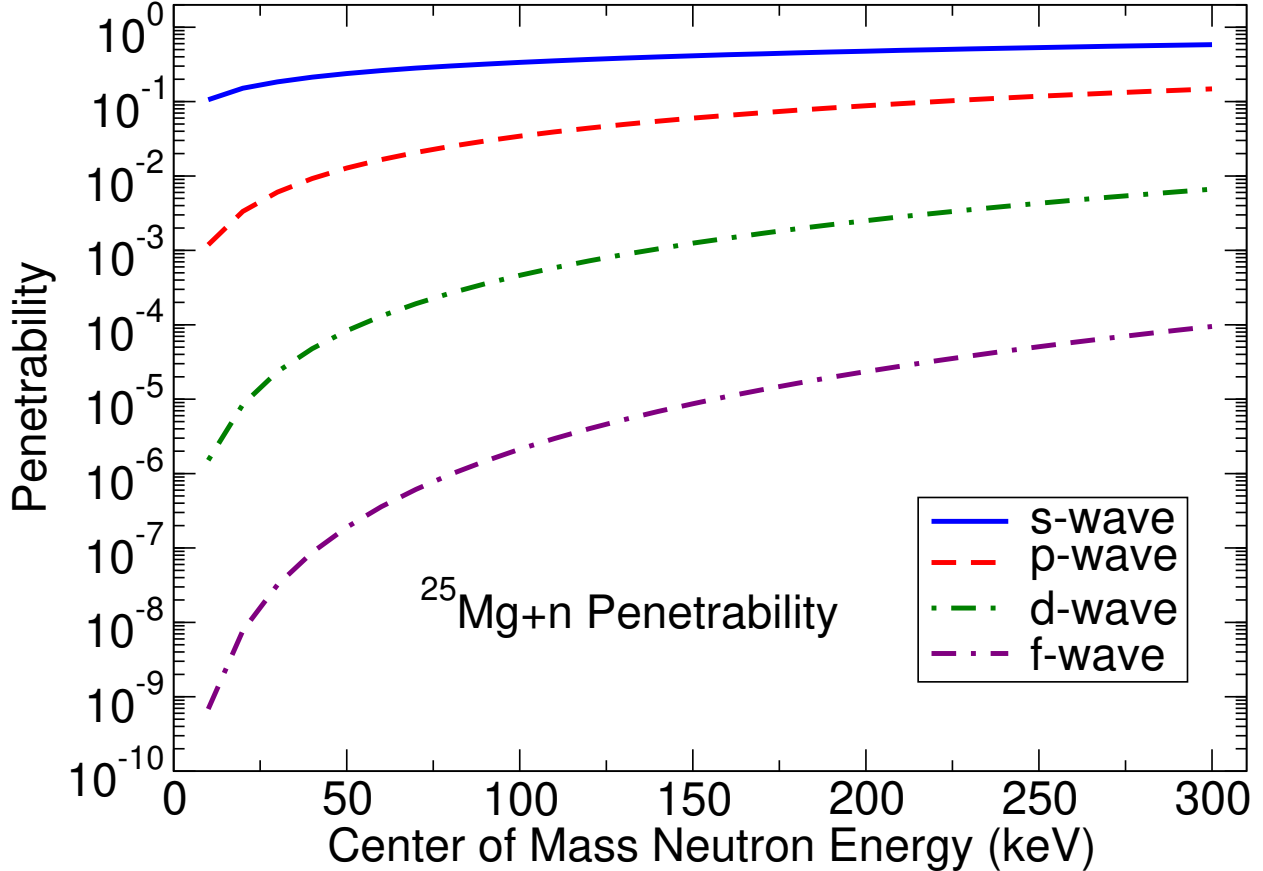


FIG. 1.  $P_\ell$  penetrability for different neutron orbital momenta  $P_\ell = 0, 1, 2, 3$  (blue solid, red dashed, green dashed-dotted, purple dot-dash-dashed, respectively) as a function of energy.

comparable to  $\Gamma_n$ , i.e.  $\Gamma_\gamma \lesssim \Gamma_n$ . This is the case for several resonances in the present case. Under this condition, the strength  $\omega\gamma$ , is directly proportional to  $\Gamma_\gamma$ ,

$$\omega\gamma = \omega \frac{\Gamma_n \cdot \Gamma_\gamma}{\Gamma_n + \Gamma_\gamma} \rightarrow \frac{\omega\Gamma_\gamma}{2} \leq \omega\gamma \leq \omega\Gamma_\gamma. \quad (3)$$

This establishes a significant difference compared to the treatment of charge particle reactions, since the single-particle strength does not affect the overall resonance strength.

Narrow resonances observed in the  $^{25}\text{Mg}(n, \gamma)^{26}\text{Mg}$  reaction therefore have either a small single-particle strength or high orbital momentum, while pronounced structures in the spectrum of a  $(d, p)$  study have a large single-particle strength. This means that unlike neutron capture, the  $(d, p)$  neutron transfer studies are not selective for narrow radiative capture resonances, but only for states with single-particle structure independent of the angular momentum. That may limit severely the usefulness for these types of surrogate reactions for predictions of neutron capture processes on short-lived nuclei in the  $r$ - or in the  $i$ -process.

The purpose of this work is to compare the results of the n-TOF  $^{25}\text{Mg}(n, \gamma)^{26}\text{Mg}$  study [15, 16] with the results of a  $^{25}\text{Mg}(d, p)^{26}\text{Mg}$  neutron transfer measurement, performed at the high-resolution Grand Raiden (GR) spectrometer [20] at the Research Center for Nuclear Physics (RCNP) in Osaka, Japan. The experiment utilized a deuteron beam of an energy of 56 MeV. This energy was chosen so that hydrogen recoils do not interfere kinematically with the  $(d, p)$  reaction protons produced by populating states in the excitation energy range of interest. At lower deuteron energies the recoil protons would generate large background in the region of interest, i.e.  $E_x > 10$  MeV, and hamper the observation of the reaction protons at the different angle settings. An additional advantage is, that for these deuteron energies, optical model parameters for the  $(d, p)$  reaction are available [21], facilitating the analysis of the experimental data.

In Sec. III the experimental details of the GR study are described, followed by a discussion of the calibration of the experimental data. In Sec. IV, calibrated spectra are examined and level parameters are deduced. This is followed, in Sec. VI, by a comparison to the results of Massimi *et al.* [16]. An  $R$ -matrix prediction for the  $^{25}\text{Mg}(n, \gamma)^{26}\text{Mg}$  reaction, based on the level parameters from the present  $^{25}\text{Mg}(d, p)^{26}\text{Mg}$  measurement, is then made. A discussion and conclusion are given in Sec. VII.

### III. EXPERIMENTAL SETUP AND PROCEDURES

The measurement of the  $^{25}\text{Mg}(d, p)^{26}\text{Mg}$  reaction was performed at RCNP using the Azimuthally Varying Field (AVF) Cyclotron, the WS beam course and the high-resolution GR spectrometer. The deuteron beam was accelerated to 56 MeV by the  $K = 140$  MeV AVF cyclotron and transported to the GR through a dispersion-matched beam line to achieve the highest resolution. [22, 23] In this mode, the resolution is limited by the resolving power of the spectrometer. Using a self-supporting  $^{25}\text{Mg}$  target (enrichment 97.8%) with a thickness of  $1 \text{ mg/cm}^2$ , a total energy resolution of about 20 keV was achieved, resulting mainly from incomplete dispersion matching, the energy loss difference of the incoming and outgoing particles, and target inhomogeneities. There is a smaller contribution from energy straggling of the scattered protons. In order to evaluate the background from reactions on carbon and oxygen target impurities, measurements were performed on a  $^{24}\text{Mg}$  target with a thickness of  $1.2 \text{ mg/cm}^2$  and Mylar foils,  $(\text{C}_{10}\text{H}_8\text{O}_4)_n$ , with a thickness of  $6 \text{ }\mu\text{m}$ . In order to measure

angular distributions, the GR was operated in three different modes:

- a) In the *0° Mode*, the spectrometer was set at 0° so that the beam enters the spectrometer along its optical axis. The magnetic field was adjusted to bend the desired excitation energy range of the protons onto the focal plane. Since the magnetic rigidity of the deuteron beam was larger compared to that of protons, the beam was bent less, and exits the first dipole (D1) at the high-momentum side (see Fig. 2). The Faraday cup consisted of two parts to allow the measurement of the current ratio. This allowed for fine adjustments of the beam location to maximize the collected beam current and minimize background. The full angular acceptance of the spectrometer was  $\pm 20$  mrad in the horizontal direction and  $\pm 40$  mrad in the vertical direction.
- b) In the *Small Angle Mode*, the cross section can be measured over spectrometer scattering angles covering the range from 2° - 6°. To stop the deuteron beam and measure the integrated current, a movable Faraday cup was located downstream of the first quadrupole.
- c) In the *Scattering Chamber Mode*, cross section measurements at scattering angles larger than 6° can be performed. In this mode, the beam is stopped and its current measured in a Faraday cup installed inside the scattering chamber.

In the *Scattering Chamber Mode*, the scattering angle can be well defined by appropriate entrance slit dimensions. In the *0° Mode* and *Small Angle Mode*, the entrance slits have to be open as much as possible. This allows the beam pass into the spectrometer for separation from the reaction products, owing to their differences in magnetic rigidity, and to minimize background from slit-edge scattering. In this situation, the scattering angle at the target  $\Theta_{scatt} = \sqrt{(\theta_{tgt}^2 + \phi_{tgt}^2)}$  can be reconstructed from measurements in the focal plane  $\theta_{fp}$  and  $\phi_{fp}$ . Here  $\theta$  and  $\phi$  refer to the horizontal and vertical scattering angle components, respectively and *fp* and *tgt* refer to the focal plane and target, respectively. To allow for a precise determination of  $\theta_{tgt}$  the angular dispersion matching condition [23] has to be fulfilled. For precise determination of the vertical angular component, we applied the overfocus mode [23] and measured the vertical position ( $y_{fp}$ ). A rectangular multi-hole aperture was used for calibration. Fig. 3 shows the measurement before (left panel) and after (right panel) calibration.

## Grand Raiden (GR)

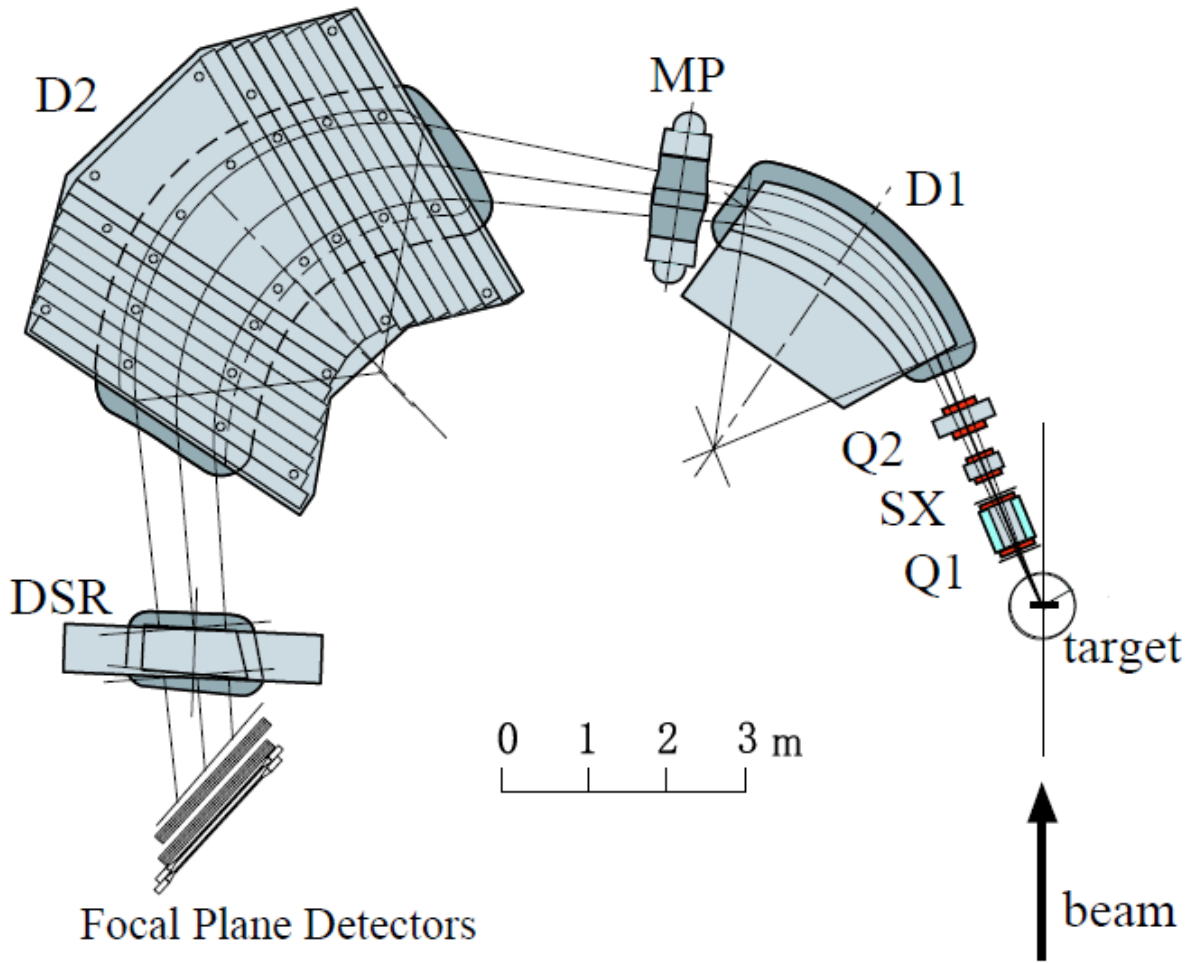


FIG. 2. Schematic view of the Grand Raiden (GR) spectrometer at RCNP [24] showing the target position (target), quadrupole magnet 1 (Q1), sextupole magnet (SX), quadrupole magnet 2 (Q2), dipole magnet 1 (D1), multipole field magnet (MP), dipole magnet 2 (D2), dipole magnet for spin rotation (DSR), and the focal plane detectors. Note that the DSR was not used for the present measurements. Further details can be found in Fujiwara *et al.* [20].

The detector system in the focal plane consisted of two Multi-Wire Drift Chambers (MWDC) both sensitive in horizontal and vertical directions. These detectors allowed for the measurements of the positions and angles in horizontal and vertical directions. Two plastic scintillation detectors with thicknesses of 3 and 10 mm were mounted downstream of the position sensitive detectors. A 10-mm-thick Al degrader was placed between the

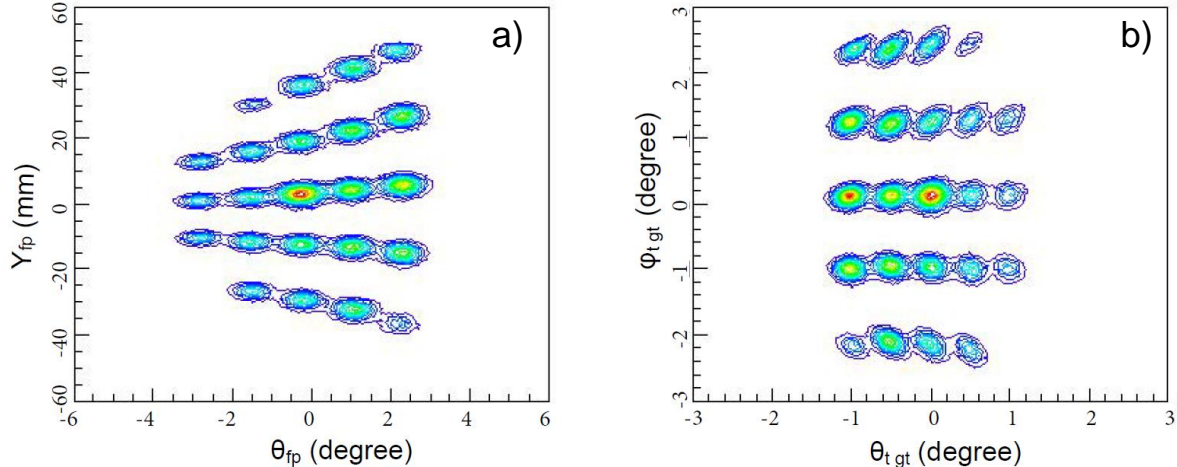


FIG. 3. Angular calibration with mult-hole slit. Left panel, a): measurement of the vertical position  $y_{fp}$  versus horizontal angle  $\phi_{fp}$ . Each spot is associated with a hole in the slit system. Right panel, b): reconstructed pattern at the target position after angular calibration. The measurement of the reaction  $^{197}\text{Au}(d, d_0)^{197}\text{Au}$  was taken at  $10^\circ$  using a target with a thickness of  $1.68 \text{ mg/cm}^2$ .

MWDCs and the scintillators to optimize the particle identification based on the  $\Delta E - E$  method. The plastic scintillation detectors also provided a fast timing signal, used to record the time-of-flight (TOF), relative to the cyclotron RF signal. The TOF spectrum was used to improve the particle identification and to reduce background.

To measure data in the excitation energy range  $E_x = 1.81 - 13 \text{ MeV}$  of the  $^{25}\text{Mg}(d, p)^{26}\text{Mg}$  reaction, three field settings of the spectrometer were necessary, owing to the limited 5% momentum acceptance of the spectrometer. The highest excitation energy setting of the spectrometer covered the range  $E_x = 8.5 - 13 \text{ MeV}$ . For this range, angular distributions were measured in the angular range of  $\theta_{c.m.} = 0^\circ - 45^\circ$ . To cover this range, three modes with Faraday cups at different locations were used, as explained above. The measurement of the beam current in the scattering chamber Faraday cup, with an electron suppression system, was the most reliable. Therefore, the other two current measurements were normalized relative to the measurement in the scattering chamber Faraday cup. This was accomplished by repeated measurements of the ratio of the currents with stable beam.

The well-separated low-lying states of  $^{26}\text{Mg}$ , with accurately known excitation energies, were used for energy calibration. For this purpose, the three spectrometer field settings

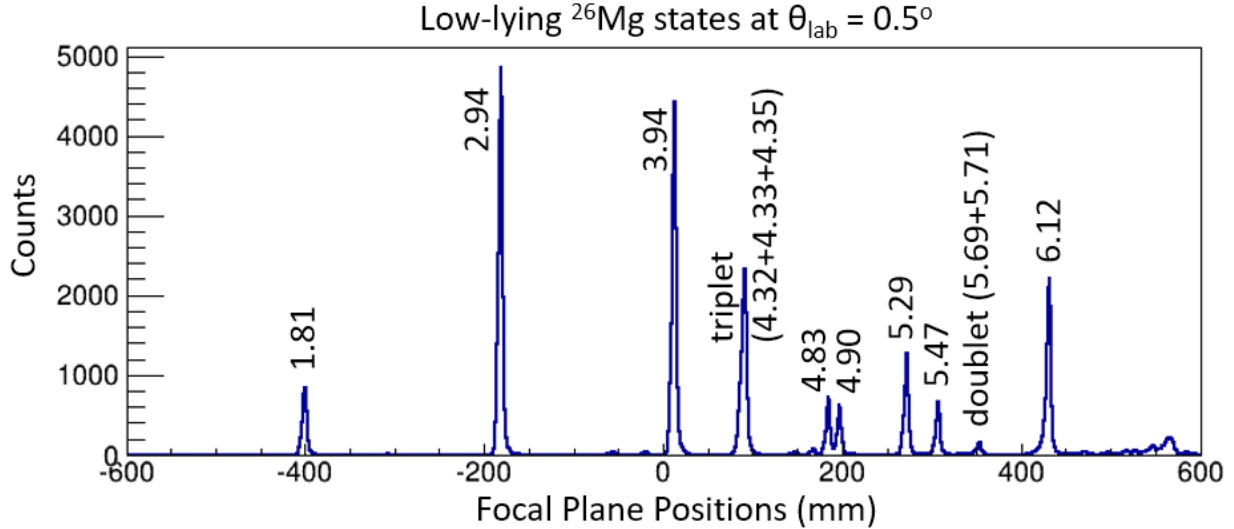


FIG. 4. Spectrum of low-lying  $^{26}\text{Mg}$  states populated by the  $^{25}\text{Mg}(d, p)^{26}\text{Mg}$  reaction at  $\theta_{\text{lab}} = 0.5^\circ$  at the low-energy setting of the spectrometer. Level energies (in MeV) are taken from Basunia and Hurst [25].

had sufficient overlap to extend the calibration of low-lying states to the higher excitation spectra. This procedure allowed for the determination of excitation energies to an accuracy of 10 - 12 keV, up to highest measured excitation energies. The resulting calibration curve is shown in Fig. 5. Note the importance of the quadratic term.

The measurement of the position and angles in the focal plane detectors allowed for the correction of higher-order aberrations. Using this procedure, resolutions of 20 - 25 keV were achieved. The corrected spectrum of the low-lying states in  $^{26}\text{Mg}$  are shown in Fig. 4. Because of the high level density, several states are not resolved despite the good resolution. For this reason, the spectra were fitted to extract the location and the number of counts of the measured peaks. The default peak fitting routine of ROOT (version 5.34.19) [26], using a right-skewed Gaussian function, was adopted for this purpose. A right-skew function was necessary because an electron energy shift occurs regularly towards the lower energy side, owing to the incomplete charge collection in the detector. The parameters of the function were obtained by fitting well isolated peaks across the focal plane and were independent from the focal plane position. Fig. 6 shows an example of the fitting, demonstrating the quality of the results. For details of the fitting, see Chen [27].

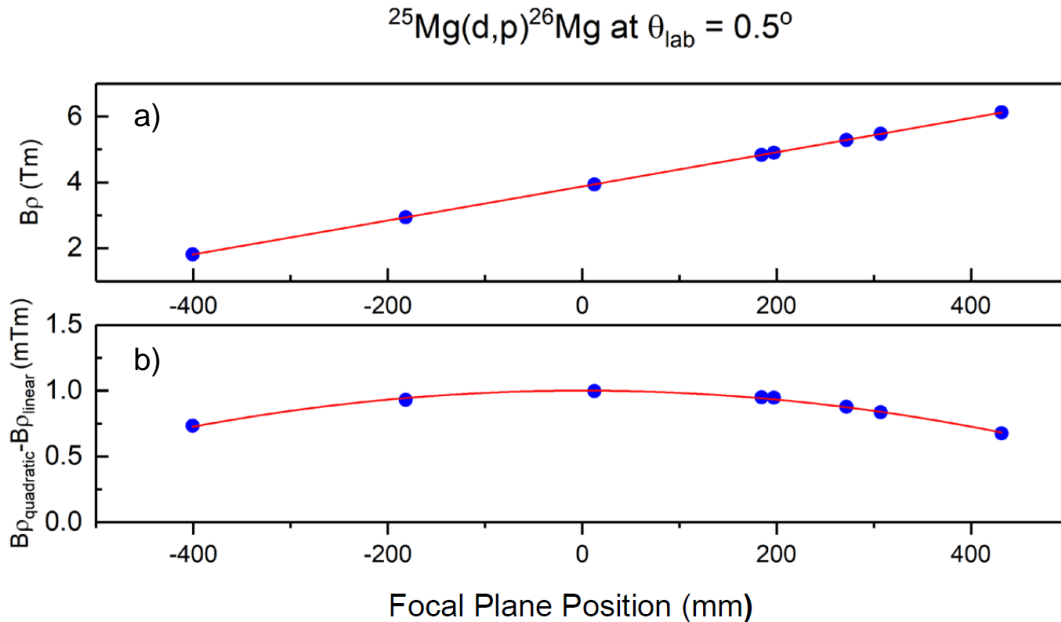


FIG. 5. Focal plane calibration. Top panel, a): quadratic fitting. Bottom panel, b): quadratic residual of the fit.

#### IV. EXPERIMENTAL RESULTS

Excited states in  $^{26}\text{Mg}$  have been measured from the  $\alpha$ -threshold at 10.61 MeV up to 1 MeV, above the neutron-threshold at 11.09 MeV, using the spectrograph setting for the highest excitation energy range. A total of 28 states have been observed and angular distributions were measured from  $0^\circ$  to  $40^\circ$  in  $5^\circ$  steps. Two typical spectra measured at  $0^\circ$  and  $30^\circ$  are shown in Fig. 7 and the resulting excitation energies are listed in Table I. The present values are in excellent agreement with the earlier results of Čujec [28], as given in Table I.

Typical angular distributions for states above the neutron threshold are shown in Fig. 8. These experimental angular distributions were analyzed in the framework of the DWBA optical model [29, 30] using the code DWUCK4 [31, 32]. This code uses the Vincent-Fortune method [33, 34] to treat transitions to particle unbound final states. The theoretical DWBA cross section is related to the experimental cross section by the usual expression [31, 35, 36]:

$$\left(\frac{d\sigma}{d\Omega}\right)_{\text{exp}} = NC^2 S_n \frac{2J_f + 1}{2J_i + 1} \frac{\sigma_{\text{DWBA}}}{2j + 1}, \quad (4)$$

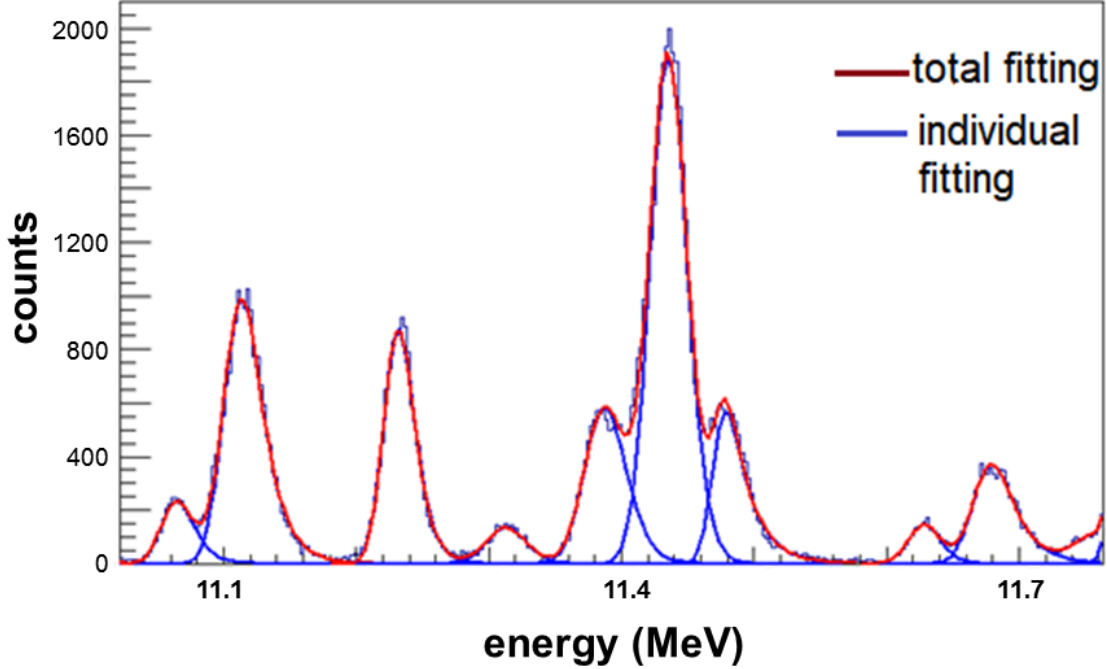


FIG. 6. Example of fitting results using a right-skewed Gaussian function.

where  $J_f$  and  $J_i$  are the spins of the final and initial state,  $j = \ell_n \pm 1/2$  the spin of the transferred neutron with orbital momentum  $\ell_n$  and  $N = 1.55$  for  $(d, p)$  reactions. The Clebsch-Gordan coefficient ( $C$ ) is unity for neutron transfer on nuclei that are not proton rich ( $Z < N$ ).

Determination of the neutron spin ( $j$ ) requires the use of a polarized deuterium beam, which was not available during the experiment because of technical issues. In its absence, the shape of the angular distributions is characterized by the orbital momentum of the transferred neutron and no information about the spin orientation can be obtained. For this reason the  $S_n$  were extracted for the most likely single neutron states,  $p_{3/2}$ ,  $d_{3/2}$  and  $f_{7/2}$ . The results for the alternative configuration differ only by a constant factor (for example, a factor of 1.19 between  $d_{5/2}$  and  $d_{3/2}$  states [36]). The optical model parameters were adapted from the extended study of  $(d, p)$  reactions at 56 MeV by Hatanaka *et al.* [21] and

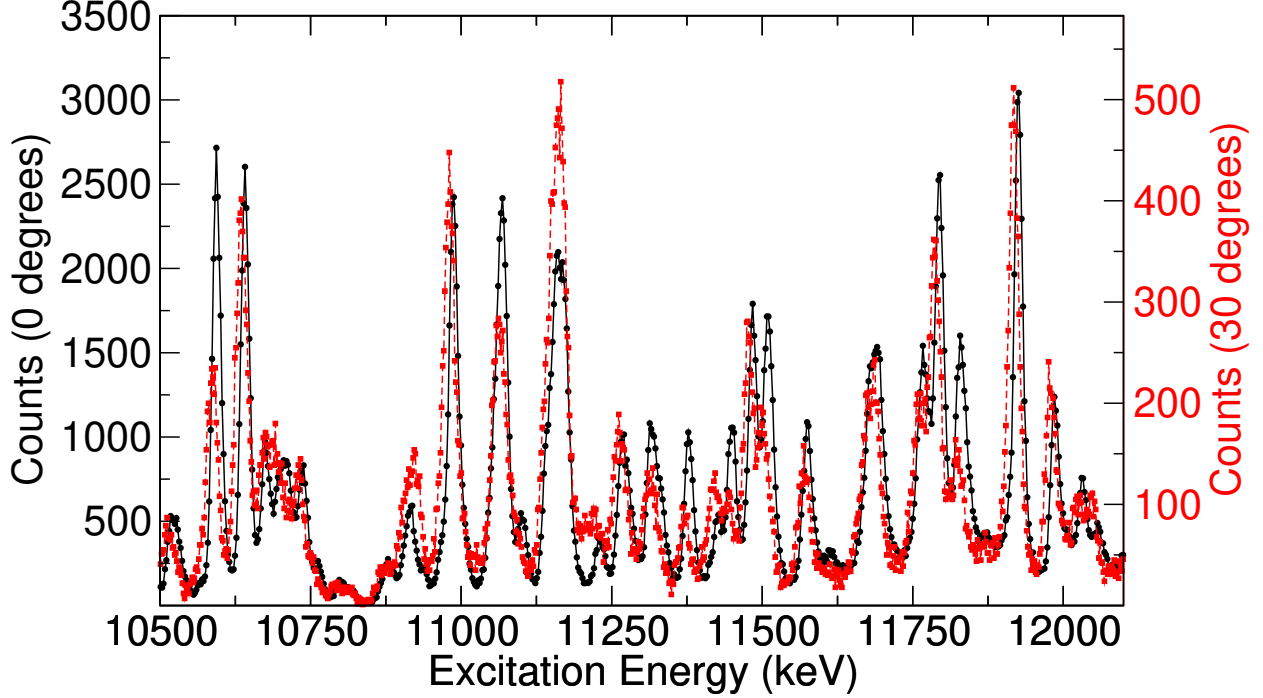


FIG. 7. Proton spectra, populating excited states in  $^{26}\text{Mg}$  from the  $\alpha$ -threshold up to 1 MeV above the neutron threshold, measured at angles of  $0^\circ$  (black circles) and  $30^\circ$  (red triangles). Shifts in the position observed for some of the peaks are well within the quoted errors for the energies.

are listed in Table II. To verify these calculations, as well as the general normalization of the experimental data, we have analyzed the  $^{12}\text{C}(d,p)^{13}\text{C}$  reaction to the final states at 3.09 MeV, 3.58 MeV and 3.85 MeV. These data were also obtained with the highest field setting of the spectrograph at all angles during our background measurements with the Mylar target. The results are in agreement with the results of Hatanaka *et al.* [21] as shown in their Figs. 3, 6 and 8.

The  $\Gamma_n$  of unbound states are correlated to  $S_n$  by [37]

$$(2J + 1)\Gamma_n = (2J + 1)S_n \cdot \Gamma_{sp}, \quad (5)$$

where  $\Gamma_{sp}$  is calculated with DWUCK4 using the same optical potential parameters as in the DWBA calculations. It should be noted that while  $S_n$ , as well as  $\Gamma_{sp}$ , are sensitive to the choice of radius, this effect is much smaller for their product as long as they are obtained with the same optical potential (see, e.g., Mao *et al.* [38]). The model dependent uncertainty is estimated to 25% and the experimental error of the cross section is 15%, mainly arising from the uncertainty of the target thickness and the charge measurements.

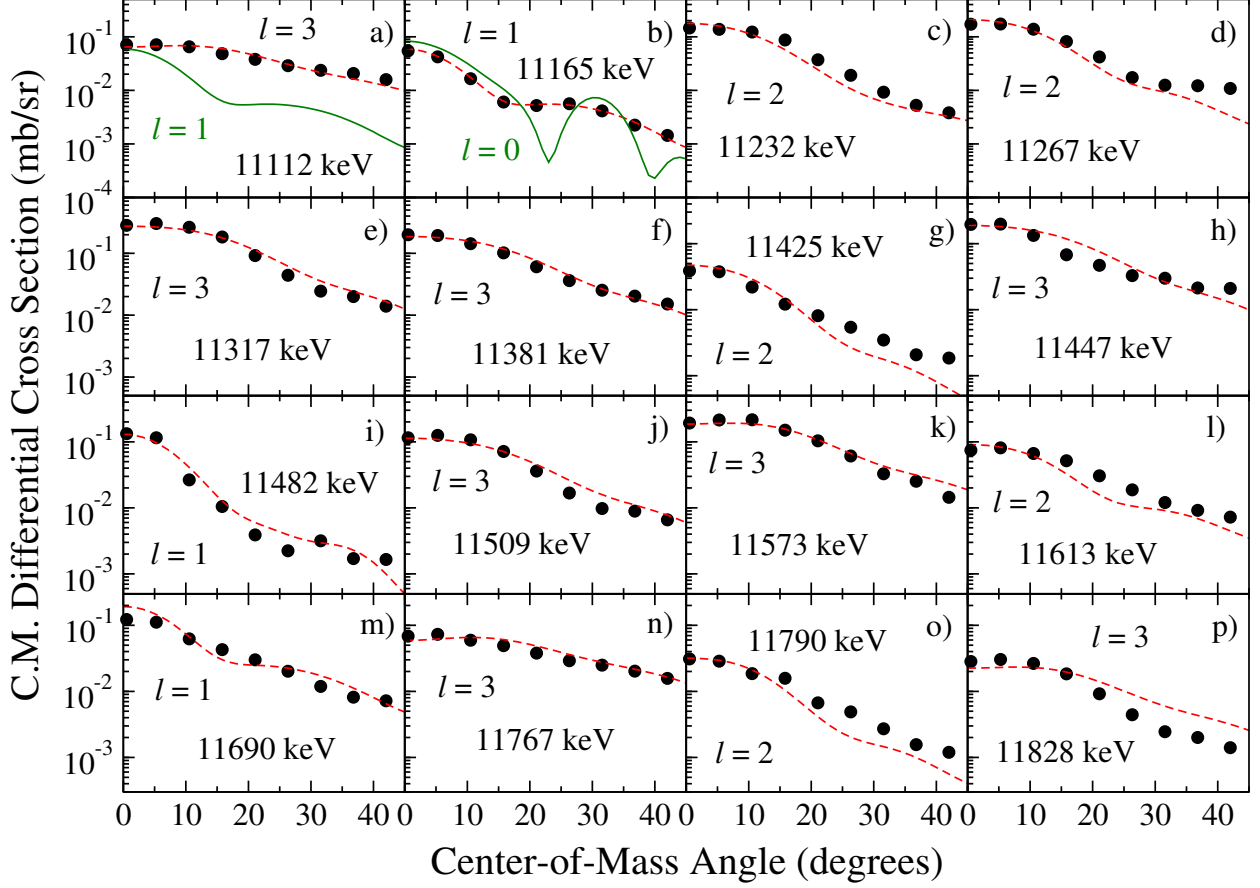


FIG. 8. Measured angular distributions (data points) and DWUCK4 calculations (solid and dashed lines) for excited states above the neutron threshold for the  $^{25}\text{Mg}(d,p)^{26}\text{Mg}$  reaction at 56 MeV incident beam energy. Here  $\ell$  is the orbital momentum of the transferred neutron. The statistical error of the data points is within the size of the symbols. In a) and b), fits using an alternative  $\ell$  (green line) are shown for comparison, while in c) through p), only the best fit (red dashed line) is shown.

## V. COMPARISON WITH $(n, \gamma)$ DATA

Calculated angular distributions together with the experimental data from this work are shown in Fig. 8. The resulting neutron orbital momenta  $\ell_n$ ,  $S_n$ , and  $\Gamma_n$  of the neutron-unbound states are listed in Table I.

The present results are compared in Table III with the  $(n, \gamma)$  results of the most recent n\_TOF experiment of Massimi *et al.* [16]. The  $S_n$  in Table III are calculated from the observed  $\Gamma_n$  and  $\ell_n$  assignments [16, 39]. This new study utilized an improved n\_TOF setup

TABLE I. Energy levels  $E_x$  of  $^{26}\text{Mg}$  and their properties.<sup>a</sup>For a discussion of the uncertainties see text.

$E_x$ (MeV) present	$E_x$ (MeV) <sup>b</sup> Čujec [28]	$\ell_n$	$(2J + 1)S_n$	$(2J + 1)\Gamma_n$ (eV)
10.641(11)	10.64	2	0.23	
10.708(10)	10.70	1	0.05	
10.808(10)		2	0.21	
10.875(11)		3	0.11	
10.915(10)	10.91	2	0.02	
10.988(11)	10.98	3	0.26	
	11.00			
11.069(10)	11.07	2	0.03	
11.112(11)	11.12	3	0.14	$2.0 \times 10^{-03}$
11.165(10)	11.16	1	0.24	$8.1 \times 10^{+03}$
11.232(10)	11.22	2	0.5	$2.3 \times 10^{+02}$
11.267(10)	11.28	2	0.03	$8.6 \times 10^{+01}$
11.317(11)	11.31	3	0.07	$3.9 \times 10^{+00}$
	11.34			
11.374(12)	11.38	3	0.08	$9.9 \times 10^{+00}$
11.425(12)		2	0.08	$1.1 \times 10^{+03}$
11.447(11)	11.45	3	0.09	$2.5 \times 10^{+01}$
11.482(10)	11.48	1	0.07	$3.9 \times 10^{+04}$
11.509(10)	11.51	3	0.11	$5.2 \times 10^{+01}$
11.573(11)	11.57	3	0.11	$8.5 \times 10^{+01}$
11.613(11)	11.63	2	0.08	$3.1 \times 10^{+03}$
11.690(10) <sup>c</sup>	11.69			
11.767(11)	11.76	3	0.13	$3.2 \times 10^{+02}$
11.790(11)	11.79	2	0.12	$9.3 \times 10^{+03}$
11.828(10)	11.83	3	0.13	$4.3 \times 10^{+02}$
11.874(11)	11.90	2	0.11	$1.1 \times 10^{+04}$
11.927(11)		3	0.16	$7.7 \times 10^{+02}$
11.981(11)		2	0.3	$4.1 \times 10^{+04}$
12.032(11)	12.00	1	0.08	$3.5 \times 10^{+05}$
12.059(12)		3	0.07	$5.2 \times 10^{+02}$

<sup>a</sup>Properties including  $\ell_n$  and  $S_n$  observed in this work. For neutron-unbound states, the  $\Gamma_n$  are also given. Excitation energies are the average of those determined at each angle where the state was observed.

<sup>b</sup>uncertainty not given

<sup>c</sup>unresolved doublet

and also performed a high precision measurement of the total neutron cross section using

TABLE II. Optical potential parameters used in the DWBA analysis of the reaction  $^{25}\text{Mg}(d, p)^{26}\text{Mg}$  [21].

Target nucleus		$V_0$ MeV	$r_0$ fm	$a_0$ fm	$W_v$ MeV	$W_D$ MeV	$r_W$ fm	$a_W$ fm	$V_{LS}$ MeV	$r_{LS}$ fm	$a_{LS}$ fm	$r_c$ fm
$^{25}\text{Mg}$	d	74.05	1.17	0.804	3.81	9.90	1.325	0.731	3.51	1.07	0.66	1.3
	p	37.57	1.144	0.69	9.88	0.0	1.32	0.657	5.6	1.01	0.6	1.25
final state		<sup>a</sup>	1.25	0.65								

<sup>a</sup>Adjusted to give the correct binding energy.

highly enriched  $^{25}\text{Mg}$ . Previous studies [14, 15] re-analyzed the total neutron cross section data of Weigmann *et al.* [40].

The state at  $E_x = 11.112(11)$  MeV shows an angular distribution of  $\ell_n = 3$  in contrast to the  $s$ -wave assignment of the 11.112 MeV state seen in Massimi *et al.* [16]. The observed  $\Gamma_n$  and  $s$ -wave character of the resonances observed by Massimi *et al.* [16] corresponds to a small  $S_n$  and is thus consistent with the absence of  $s$ -wave states in the present experiment (see Table I). For this reason we assign the level observed in the present  $(d, p)$  experiment to the new 11.102(1) MeV state observed in the high-resolution  $(d, d')$  and  $(p, p')$  studies of Adsley *et al.* [13].

In the energy region of the  $p$ -wave state at  $E_x = 11.165(10)$  MeV, Massimi *et al.* [16] observe two states at  $E_x = 11.163$  MeV and 11.169 MeV, which were not resolved in our experiment. The  $S_n$  of additional states at  $E_x = 11.154$  MeV and 11.171 MeV are too small to be populated in the present  $(d, p)$  experiment. We assign this state to that at  $E_x = 11.169$  MeV observed by Massimi *et al.* [16] because both have a  $p$ -wave character and similar  $S_n$  (0.24 and 0.37). In contrast, the state at  $E_x = 11.163$  MeV has been assigned  $\ell_n = 0$  by Massimi *et al.* [16], while our angular distribution (Fig. 8) shows that any  $s$ -wave strength is significantly lower than that of the  $p$ -wave. This is in agreement with its small  $S_n$  (Table III).

A state at  $E_x = 11.119$  MeV has been observed by Massimi *et al.* [16]. The  $\Gamma_n$  of this state is 5.2 keV, which corresponds to a small  $S_n$  because of the  $\ell_n$  assignment (see Table III) and might be too weak to be observed in the  $(d, p)$  reaction.

The state at  $E_x = 11.232(10)$  MeV can only correspond to the  $E_x = 11.243$  MeV state in Massimi *et al.* [16] on the basis of energy alone. No other states have been observed within a  $2\sigma$  energy uncertainty. However, the  $(d, p)$  data show an  $\ell_n$  value of 2 (see Fig. 8), whereas Massimi *et al.* [16] assigned a spin of  $2^-$  and  $\ell_n = 1$  to this state. This could indicate that either these are two different states or one that the  $\ell_n$  assignment is in error.

The state at  $E_x = 11.267(10)$  MeV could in principle correspond to five states seen in Massimi *et al.* [16] at energies between  $E_x = 11.274$  MeV and 11.295 MeV, which could not be resolved because of the limited energy resolution of 20-25 keV in the present  $(d, p)$  experiment. Two of the states have small  $\Gamma_n$ , which correspond to  $(2J + 1)S_n < 0.01$ , indicating that they cannot be observed in the  $(d, p)$  reaction. The other remaining states might be an unresolved multiplet in the  $(d, p)$  reaction. The large deviation of the angular distribution data at backward angles (see Fig. 8) supports this interpretation.

No counterpart of the  $E_x = 11.317(11)$  MeV state can be found in the  $(n, \gamma)$  data [16]. None of these states have an  $f$ -wave structure and its  $\Gamma_n$  determined from the  $S_n$  is at the low end of widths observed in  $(n, \gamma)$  measurements (see Table III). The energetically closest state within the errors is the  $p$ -wave states at  $E_x = 11.328$  MeV. However, the  $S_n$  of this state is too small to be observed in the present experiment. The high resolution elastic scattering experiments of Adsley *et al.* [13] report two states at  $E_x = 11.321(1)$  MeV and 11.329(1) MeV, which could be the counterparts of the 11.317 MeV state observed in the  $(d, p)$  reaction and the 11.328 MeV state seen in the  $(n, \gamma)$  reaction.

The  $E_x = 11.329(1)$  MeV state is of astrophysical importance because it corresponds to the lowest resonance at  $E_\alpha^{\text{c.m.}} = 704$  keV in the  $^{22}\text{Ne}(\alpha, n)$  and  $(\alpha, \gamma)$  reactions. The weighted average of all reported resonance energies [41–47] corresponds to an excitation energy of 11.318(2) MeV. This state has not been observed in any of the reported  $(n, \gamma)$  measurements within a  $3\sigma$  error in energy [14–16]. The ratio of the reported resonance strengths in both reaction channels leads to a ratio of  $\Gamma_\gamma/\Gamma_n \approx 0.3$ . The known  $\gamma$ -decay scheme of the resonance [41, 46, 47], together with the recommended upper limits for the  $\gamma$ -strength in this mass region [48], leads to a  $\Gamma_\gamma$  on the order of  $\approx 1$  eV and smaller. This is in agreement with the  $\Gamma_\gamma$  observed in the  $(n, \gamma)$  study of Massimi *et al.* [16], which favors a large  $\Gamma_\gamma$ .

Combining this result with the experimental ratio of the widths leads to  $\Gamma_n \approx 1$  eV for this resonance. This is in good agreement with a  $\Gamma_n$  of  $(2J+1)\Gamma_n = 4$  eV for the  $E_x = 11.317$  MeV

level observed in the present experiment. In addition, the energy falls within the uncertainty of the present measurement and no other suitable state is known that might correspond to the  $E_{\alpha}^{\text{c.m.}} = 704$  keV resonance. For this reason we conclude the  $E_x = 11.317$  MeV state corresponds to the  $E_{\alpha}^{\text{c.m.}} = 704$  keV resonance in the  $^{22}\text{Ne}(\alpha, n)$  and  $(\alpha, \gamma)$  reactions. The spin of the resonance has to have natural parity and the parity has to be negative because of the  $f$ -wave character of the  $E_x = 11.317$  MeV state. Spins  $>1$  can be excluded on penetrability arguments. For example, a spin of  $3^-$  would exceed the Wigner limit by a factor of  $\approx 6$ . As a result, the spin parity assignment of this resonance has to be  $1^-$ . Possible explanations for the differences between the results of the  $(d, p)$ - and the  $(n, \gamma)$ - reactions are discussed in Sec. VII.

TABLE III. Comparison of  $^{26}\text{Mg}$  states populated by the  $(n,\gamma)$  reaction

This work				Massimi <i>et. al</i> [16, 39]				
$E_x$	$\ell_n$	$(2J+1)\Gamma_n$	$(2J+1)S_n$	$E_x^1$	$\ell_n$	$J^\pi$	$\Gamma_n$	$(2J+1)S_n$
(MeV)		(eV)		(MeV)			(eV)	
11.112(11)	3	0.002	0.14	11.112	0	$2^+$	2095	0.02
				11.154	2	$1^+$	7	0.1
11.165(10)	1	8140	0.24	11.163	0	$2^+$	5310	0.06
				11.169	1	$3^-$	1940	0.37
				11.171			1-30	small
				11.190	0	$3^+$	5230	0.05
11.232(10)	2	230	0.5	11.243	1	$2^-$	5950	0.11
				11.274	0	$2^+$	410	0.002
				11.280	1	$3^-$	1810	0.08
11.267(10)	2	86	0.03	11.285	1	$2^-$	1030	0.03
				11.289			3-20	small
				11.295	1	$2^-$	7370	0.21
11.317(11)	3	4	0.07	11.328	1	$3^-$	114	0.004

<sup>1</sup> Errors less than 0.1 keV.

## VI. $R$ -MATRIX CROSS SECTION COMPARISONS

With the level parameters of states in  $^{26}\text{Mg}$ , determined in this work by way of the  $^{25}\text{Mg}(d,p)^{26}\text{Mg}$  reaction, it is now interesting to compare with direct measurements of  $^{25}\text{Mg}(n,\gamma)^{26}\text{Mg}$  cross section. However, even direct measurements of the  $^{25}\text{Mg}(n,\gamma)^{26}\text{Mg}$  reaction still only report yields, which contain target effects that distort them significantly from the underlying cross section. Therefore, the comparison is made using phenomenological  $R$ -matrix theory. For the level parameters of the present work, this comparison is facilitated by the Brune formalism [49]. This alternate parameterization allows for experimentally measured energies and widths to be input directly into the  $R$ -matrix analysis.

Conveniently, the recent measurement of Massimi *et al.* [16] also give the physical parameters resulting from their  $R$ -matrix fit. The  $R$ -matrix code AZURE2 [50, 51] was used for the present calculations. Channel radii of 5.5 fm were used for both the  $\alpha$ -particle and neutron particle pairs. Conveniently, the Brune formalism also eliminates the use of boundary conditions [49].

The level parameters used for the comparison calculation from the present work and those from Massimi *et al.* [16] are given in Table IV. Note that only the levels of Massimi *et al.* [16] with a given  $J^\pi$  were used for the calculations, but this does not substantially affect the comparison. The cross section comparison is shown in Fig. 9. A rather poor reproduction of the  $^{25}\text{Mg}(n, \gamma)^{26}\text{Mg}$  cross section of Massimi *et al.* [16] is obtained with the level parameters from the present  $^{25}\text{Mg}(d, p)^{26}\text{Mg}$  study.

## VII. DISCUSSION AND CONCLUSION

The present study demonstrates that the application of  $(d, p)$  transfer reaction measurements is not necessarily a suitable or sufficient approach for extracting neutron capture reaction rates. In the case of the  $^{25}\text{Mg}(n, \gamma)^{26}\text{Mg}$  reaction, representing neutron capture on light (e.g.  $sd$ -shell) stable nuclei, the neutron threshold is around 10 MeV and the compound nucleus level density at this excitation energy range is rather high ( $\approx 50$  states per 1 MeV). Yet the data indicate only a few single-particle states. The reason for this is that most of the single-particle strength sum rule has been exhausted by states at lower excitation energies. The three low-lying  $s$ -wave states in  $^{26}\text{Mg}$  already exhaust more than 50% of the sum rule  $(2J + 1)\Gamma_n = 12$  [36]. Therefore, only a limited number of resonances appear in the energy range of astrophysical relevance. Little or no correlation can be seen between the resonances observed in the  $(n, \gamma)$  reaction and the states identified in the present  $(d, p)$  experiment. A similar observation has been made by Liljestr and *et al.* [52] for the case of the  $^{32}\text{S}(d, p)^{33}\text{S}$  reaction. There are several reasons for this, which are discussed below.

Reactions like  $^{25}\text{Mg}(n, \gamma)^{26}\text{Mg}$  are mainly sensitive to  $s$ - and  $p$ -wave capture into states with a pronounced  $\gamma$ -strength. Neutron capture for higher  $\ell$  value neutrons is reduced because of their reduced neutron penetrabilities (see Fig. 1), especially in the first few hundred keV above the threshold. On the other hand, the  $(d, p)$  reactions are limited in sensitivity to the population of states with large  $S_n$ . Typical experimental lower limits are

TABLE IV. Level parameters used for the  $R$ -matrix comparison calculation shown in Fig. 9. The range of  $J^\pi$  values are constrained by the measured orbital angular momentum of the present experiment.

Level Energy (MeV)	$J^\pi$	$\Gamma_\gamma$ (eV)	$\Gamma_n$ (eV)
<b>This Work</b>			
11.112	$(0-6)^-$	1	$2 \times 10^{-3}$
11.165	$(1-4)^-$	3.3	1160
11.232	$(0-5)^+$	3	230
11.267	$(0-5)^+$	3	86
11.317	$(0-6)^-$	1.33	0.4
<b>Massimi <i>et al.</i> [16]</b>			
11.112	$2^+$	1.37	2095
11.154	$1^+$	4.4	7
11.163	$2^+$	2.8	5310
11.169	$3^-$	3.3	1940
11.190	$3^+$	1.3	5230
11.243	$2^-$	4.7	5950
11.274	$2^+$	2.2	410
11.280	$3^-$	0.3	1810
11.285	$2^-$	4.8	1030
11.295	$2^-$	6.6	7370

about 0.05 to 0.1, depending on the experimental conditions, like energy resolution and solid angle. As a consequence,  $s$ -wave resonances with  $\Gamma_n$  in the few keV range correspond to  $S_n$  too small to be observed in a neutron transfer reaction. On the other hand, states observed in the  $(d, p)$  reaction can have a  $\Gamma_\gamma$  too small to be observed in neutron induced reactions ( $\lesssim 1$  eV).

The  $(d, p)$  transfer reactions preferentially populate pronounced single-particle states, while radiative neutron capture resonances correspond to levels with dominant  $\gamma$ -decay strength. Unbound single-particle states will appear as broad resonances. This width can

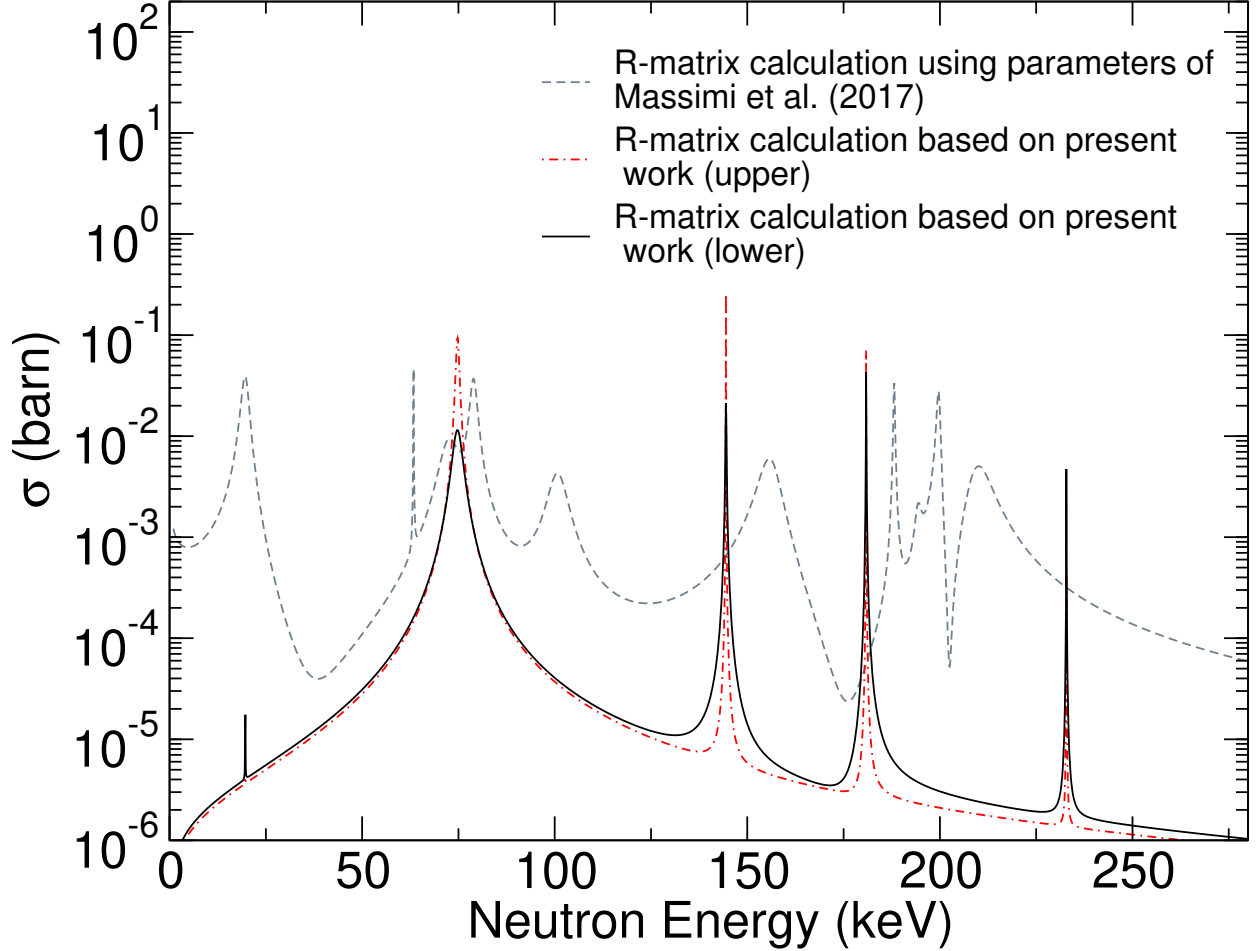


FIG. 9. Comparison of the cross section for the  $^{25}\text{Mg}(n, \gamma)^{26}\text{Mg}$  reaction calculated from the  $R$ -matrix parameters of Massimi *et al.* [16] (grey dashed line) versus the upper (red dash-dotted line) and lower limits (black solid line) calculated using the level parameters of the present work and the range of allowed angular momentum. Calculations were performed using the code AZURE2.

be several keV to hundreds of keV depending on  $S_n$ , and therefore primarily add through their broad tail contributions to the overall cross section behavior at a level corresponding to their  $\Gamma_\gamma$ . It is, therefore, important to obtain information about the strength of the  $\gamma$ -decay channel of the specific resonance states, via, e.g., a study of the  $(d, p - \gamma)$  reaction.

The impact of the  $\gamma$ -strength is amplified for medium mass nuclei with high-level density, where the cross section does not depend on the nuclear structure configuration of individual resonance states as in the present case for  $^{26}\text{Mg}$ . The statistical model [53] suggests that the cross section is largely determined by the  $\gamma$ -strength function [54] and scales with the level density. While the high level-density removes the uncertainty due to the difference

in selection and population of resonance states in the two methods, the overall reaction strength is still dominated by the  $\gamma$ -channel, as demonstrated in a recent study [55].

Because of the differences in population probability of  $(d, p)$  and  $(n, \gamma)$  reactions on nuclei with high neutron thresholds,  $(d, p)$  reactions are in most cases poorly suited to predict the cross section of radiative neutron capture reactions. At least in cases where the cross section is dominated by individual resonances. On the other hand, both reactions are rather complimentary to one another and together provide a valuable approach for exploring the structure of neutron unbound states in compound nuclei near and far from stability.

## ACKNOWLEDGMENTS

This research utilized resources from the Notre Dame Center for Research Computing and was supported by the National Science Foundation through Grant No. Phys-0758100, and the Joint Institute for Nuclear Astrophysics through Grant No. Phys-0822648 and PHY-1430152 (JINA Center for the Evolution of the Elements).

- 
- [1] F. Käppeler, R. Gallino, S. Bisterzo, and W. Aoki, *Rev. Mod. Phys.* **83**, 157 (2011).
  - [2] J. B. Dragt, J. W. M. Dekker, H. Gruppelaar, and A. J. Janssen, *Nuclear Science and Engineering* **62**, 117 (1977), <https://doi.org/10.13182/NSE77-3>.
  - [3] I. Leya and J. Masarik, *Meteoritics & Planetary Science* **48**, 665 (2013), <https://onlinelibrary.wiley.com/doi/pdf/10.1111/maps.12090>.
  - [4] Y. A. Litvinov, T. Sthlker, X. W. Ma, Y. H. Zhang, and T. Yamaguchi, *Journal of Physics: Conference Series* **1401**, 012001 (2020).
  - [5] J. E. Escher, J. T. Burke, F. S. Dietrich, N. D. Scielzo, I. J. Thompson, and W. Younes, *Rev. Mod. Phys.* **84**, 353 (2012).
  - [6] J. E. Escher, J. T. Burke, R. O. Hughes, N. D. Scielzo, R. J. Casperson, S. Ota, H. I. Park, A. Saastamoinen, and T. J. Ross, *Phys. Rev. Lett.* **121**, 052501 (2018).
  - [7] A. M. Mukhamedzhanov, F. M. Nunes, and P. Mohr, *Phys. Rev. C* **77**, 051601(R) (2008).
  - [8] W. Huang, G. Audi, M. Wang, F. G. Kondev, S. Naimi, and X. Xu, *Chinese Physics C* **41**, 030002 (2017).

- [9] M. Wang, G. Audi, F. G. Kondev, W. Huang, S. Naimi, and X. Xu, *Chinese Physics C* **41**, 030003 (2017).
- [10] R. Longland, C. Iliadis, and A. I. Karakas, *Phys. Rev. C* **85**, 065809 (2012).
- [11] R. Talwar, T. Adachi, G. P. A. Berg, L. Bin, S. Bisterzo, M. Couder, R. J. deBoer, X. Fang, H. Fujita, Y. Fujita, J. Görres, K. Hatanaka, T. Itoh, T. Kadoya, A. Long, K. Miki, D. Patel, M. Pignatari, Y. Shimbara, A. Tamii, M. Wiescher, T. Yamamoto, and M. Yosoi, *Phys. Rev. C* **93**, 055803 (2016).
- [12] H. Jayatissa, G. Rogachev, V. Goldberg, E. Koshchiy, G. Christian, J. Hooker, S. Ota, B. Roeder, A. Saastamoinen, O. Trippella, S. Upadhyayula, and E. Uberseder, *Physics Letters B* **802**, 135267 (2020).
- [13] P. Adsley, J. W. Brümmner, T. Faestermann, S. P. Fox, F. Hammache, R. Hertenberg, A. Meyer, R. Neveling, D. Seiler, N. de Séréville, and H.-F. Wirth, *Phys. Rev. C* **97**, 045807 (2018).
- [14] P. E. Koehler, *Phys. Rev. C* **66**, 055805 (2002).
- [15] C. Massimi, P. Koehler, S. Bisterzo, N. Colonna, R. Gallino, F. Gunsing, F. Käppeler, G. Lorusso, A. Mengoni, M. Pignatari, G. Vannini, U. Abbondanno, G. Aerts, H. Álvarez, F. Álvarez-Velarde, S. Andriamonje, J. Andrzejewski, P. Assimakopoulos, L. Audouin, G. Badurek, M. Barbagallo, P. Baumann, F. Bečvář, F. Belloni, M. Bennett, E. Berthoumieux, M. Calviani, F. Calviño, D. Cano-Ott, R. Capote, C. Carrapiço, A. Carrillo de Albornoz, P. Cennini, V. Chepel, E. Chiaveri, G. Cortes, A. Couture, J. Cox, M. Dahlfors, S. David, I. Dillmann, R. Dolfini, C. Domingo-Pardo, W. Dridi, I. Duran, C. Eleftheriadis, M. Embid-Segura, L. Ferrant, A. Ferrari, R. Ferreira-Marques, L. Fitzpatrick, H. Fraiss-Koelbl, K. Fujii, W. Furman, I. Goncalves, E. González-Romero, A. Goverdovski, F. Gramegna, E. Griesmayer, C. Guerrero, B. Haas, R. Haight, M. Heil, A. Herrera-Martinez, F. Herwig, R. Hirschi, M. Igashira, S. Isaev, E. Jericha, Y. Kadi, D. Karadimos, D. Karamanis, M. Kerveno, V. Ketlerov, V. Konovalov, S. Kopecky, E. Kossionides, M. Krtička, C. Lampoudis, H. Leeb, C. Lederer, A. Lindote, I. Lopes, R. Losito, M. Lozano, S. Lukic, J. Marganiec, L. Marques, S. Marrone, T. Martínez, P. Mastinu, E. Mendoza, P. M. Milazzo, C. Moreau, M. Mosconi, F. Neves, H. Oberhummer, S. O'Brien, M. Oshima, J. Pancin, C. Papachristodoulou, C. Papadopoulos, C. Paradela, N. Patronis, A. Pavlik, P. Pavlopoulos, L. Perrot, M. T. Pigni, R. Plag, A. Plompen, A. Plukis, A. Poch, J. Praena, C. Pretel, J. Quesada, T. Rauscher,

- R. Reifarth, G. Rockefeller, M. Rosetti, C. Rubbia, G. Rudolf, J. Salgado, C. Santos, L. Sarchiapone, R. Sarmiento, I. Savvidis, C. Stephan, G. Tagliente, J. L. Tain, D. Tarrío, L. Tassan-Got, L. Tavora, R. Terlizzi, P. Vaz, A. Ventura, D. Villamarin, V. Vlachoudis, R. Vlastou, F. Voss, S. Walter, H. Wendler, M. Wiescher, and K. Wisshak (n\_TOF Collaboration), *Phys. Rev. C* **85**, 044615 (2012).
- [16] C. Massimi, S. Altstadt, J. Andrzejewski, L. Audouin, M. Barbagallo, V. Bàcares, F. Beçvâê, F. Belloni, E. Berthoumieux, J. Billowes, S. Bisterzo, D. Bosnar, M. Brugger, M. Calviani, F. Calviño, D. Cano-Ott, C. Carrapiço, D. Castelluccio, F. Cerutti, E. Chiaveri, L. Cosentino, M. Chin, G. Clai, N. Colonna, G. Cortés, M. Cortés-Giraldo, S. Cristallo, M. Diakaki, C. Domingo-Pardo, I. Duran, R. Dressler, C. Eleftheriadis, A. Ferrari, P. Finocchiaro, K. Fraival, S. Ganesan, A. García, G. Giubrone, I. Gonçalves, E. González-Romero, E. Griesmayer, C. Guerrero, F. Gunsing, A. Hernández-Prieto, D. Jenkins, E. Jericha, Y. Kadi, F. Käppeler, D. Karadimos, N. Kivel, P. Koehler, M. Kokkoris, S. Kopecky, M. Krtička, J. Kroll, C. Lampoudis, C. Langer, E. Leal-Cidoncha, C. Lederer, H. Leeb, L. Leong, S. L. Meo, R. Losito, A. Mallick, A. Manousos, J. Marganec, T. Martínez, P. Mastinu, M. Mastromarco, E. Mendoza, A. Mengoni, P. Milazzo, F. Mingrone, M. Mirea, W. Mondelaers, A. Musumarra, C. Paradela, A. Pavlik, J. Perkowski, M. Pignatari, L. Piersanti, A. Plompen, J. Praena, J. Quesada, T. Rauscher, R. Reifarth, A. Riego, M. Robles, C. Rubbia, M. Sabaté-Gilarte, R. Sarmiento, A. Saxena, P. Schillebeeckx, S. Schmidt, D. Schumann, G. Tagliente, J. Tain, D. Tarrío, L. Tassan-Got, A. Tsinganis, S. Valenta, G. Vannini, I. V. Rijs, V. Variiale, P. Vaz, A. Ventura, M. Vermeulen, V. Vlachoudis, R. Vlastou, A. Wallner, T. Ware, M. Weigand, C. Weiß, R. Wynants, T. Wright, and P. Žugec, *Physics Letters B* **768**, 1 (2017).
- [17] N. Larson, *Updated Users' Guide for SAMMY: Multilevel R-matrix Fits to Neutron Data Using Bayes' Equations*, Tech. Rep. (Oak Ridge National Laboratory, 2008) SAMMY, Computer Code, Report No. ORNL/TM-9179/R8.
- [18] H. Schatz, A. Aprahamian, J. Görres, M. Wiescher, T. Rauscher, J. Rembges, F.-K. Thielemann, B. Pfeiffer, P. Möller, K.-L. Kratz, H. Herndl, B. Brown, and H. Rebel, *Physics Reports* **294**, 167 (1998).
- [19] H. E. Gove, in *Nuclear Reactions*, Vol. 1, edited by P. M. Endt and M. Demeur (1959) p. 259.
- [20] M. Fujiwara, H. Akimune, I. Daito, H. Fujimura, Y. Fujita, K. Hatanaka, H. Ikegami,

- I. Katayama, K. Nagayama, N. Matsuoka, S. Morinobu, T. Noro, M. Yoshimura, H. Sakaguchi, Y. Sakemi, A. Tamii, and M. Yosoi, *Nuclear Instruments and Methods in Physics Research Section A: Accelerators, Spectrometers, Detectors and Associated Equipment* **422**, 484 (1999).
- [21] K. Hatanaka, N. Matsuoka, T. Saito, K. Hosono, M. Kondo, S. Kato, T. Higo, S. Matsuki, Y. Kadota, and K. Ogino, *Nuclear Physics A* **419**, 530 (1984).
- [22] D. Hendrie, *Nuclear Spectroscopy and Reactions, Part A*, edited by J. Cerny (Academic Press, New York, 1974).
- [23] H. Fujita and Y. Fujita and G.P.A. Berg and A.D. Bacher and C.C. Foster and K. Hara and K. Hatanaka and T. Kawabata and T. Noro and H. Sakaguchi and Y. Shimbara and T. Shinada and E.J. Stephenson and H. Ueno and M. Yosoi, *Nucl. Instr. Meth. Phys. Res. A: Accelerators, Spectrometers, Detectors and Associated Equipment* **484**, 17 (2002).
- [24] M. Yosoi, *Structures and fragmentations of the deep-hole states in  $^{11}\text{B}$  and  $^{15}\text{N}$* , Ph.D. thesis, Kyoto University (2003).
- [25] M. Basunia and A. Hurst, *Nuclear Data Sheets* **134**, 1 (2016).
- [26] R. Brun and F. Rademakers, *Nuclear Instruments and Methods in Physics Research Section A: Accelerators, Spectrometers, Detectors and Associated Equipment* **389**, 81 (1997), new Computing Techniques in Physics Research V.
- [27] Y. Chen, *Study of High Energy Levels of  $^{26}\text{Mg}$  through the  $(d, p)$  Reaction and Its Implications for the Neutron Source in Nuclear Astrophysics*, Ph.D. thesis, University of Notre Dame (2019).
- [28] B. Čujec, *Phys. Rev.* **136**, B1305 (1964).
- [29] P. E. Hodgson, *Nuclear reactions and nuclear structure*, International series of monographs on physics (Oxford, England) (Clarendon Press, Oxford, 1971).
- [30] G. R. Satchler, *Direct nuclear reactions*, International series of monographs on physics (Oxford, England) ; 68 (Clarendon Press ; Oxford University Press, Oxford : New York, 1983).
- [31] P.D.Kunz, “Zero range distorted wave approximation,” unpublished, University of Colorado (1973).
- [32] P. D. Kunz and E. Rost, “The distorted-wave born approximation,” in *Computational Nuclear Physics 2: Nuclear Reactions*, edited by K. Langanke, J. A. Maruhn, and S. E. Koonin (Springer New York, New York, NY, 1993) pp. 88–107.
- [33] C. M. Vincent and H. T. Fortune, *Phys. Rev. C* **2**, 782 (1970).

- [34] C. M. Vincent and H. T. Fortune, *Phys. Rev. C* **7**, 865 (1973).
- [35] M. Burlein, K. S. Dhuga, and H. T. Fortune, *Phys. Rev. C* **29**, 2013 (1984).
- [36] H. Arciszewski, E. Bakkum, C. Van Engelen, P. Endt, and R. Kamermans, *Nuclear Physics, Section A* **430**, 234 (1984).
- [37] J. Schiffer, *Nuclear Physics* **46**, 246 (1963).
- [38] Z. Q. Mao, H. T. Fortune, and A. G. Lacaze, *Phys. Rev. C* **53**, 1197 (1996).
- [39] C. Massimi, private communication (2016).
- [40] H. Weigmann, R. L. Macklin, and J. A. Harvey, *Phys. Rev. C* **14**, 1328 (1976).
- [41] K. Wolke, V. Harms, H. W. Becker, J. W. Hammer, K. L. Kratz, C. Rolfs, U. Schröder, H. P. Trautvetter, M. Wiescher, and A. Wöhr, *Zeitschrift für Physik A Atomic Nuclei* **334**, 491 (1989).
- [42] V. Harms, K.-L. Kratz, and M. Wiescher, *Phys. Rev. C* **43**, 2849 (1991).
- [43] H. Drotleff, A. Denker, H. Knee, M. Soine, G. Wolf, J. Hammer, U. Griefe, C. Rolfs, and H. Trautvetter, *Astrophysical Journal* **414**, 735 (1993).
- [44] U. Giesen, C. Browne, J. Görres, S. Graff, C. Iliadis, H.-P. Trautvetter, M. Wiescher, W. Harms, K. Kratz, B. Pfeiffer, R. Azuma, M. Buckby, and J. King, *Nuclear Physics A* **561**, 95 (1993).
- [45] M. Jaeger, R. Kunz, A. Mayer, J. W. Hammer, G. Staudt, K. L. Kratz, and B. Pfeiffer, *Phys. Rev. Lett.* **87**, 202501 (2001).
- [46] M. Jaeger, Ph.D. thesis, U. Stuttgart (2001).
- [47] S. Hunt, C. Iliadis, A. Champagne, L. Downen, and A. Cooper, *Phys. Rev. C* **99**, 045804 (2019).
- [48] P. Endt, *Atomic Data and Nuclear Data Tables* **55**, 171 (1993).
- [49] C. R. Brune, *Phys. Rev. C* **66**, 044611 (2002).
- [50] R. E. Azuma, E. Uberseder, E. C. Simpson, C. R. Brune, H. Costantini, R. J. de Boer, J. Görres, M. Heil, P. J. LeBlanc, C. Ugalde, and M. Wiescher, *Phys. Rev. C* **81**, 045805 (2010).
- [51] E. Uberseder and R. J. deBoer, *AZURE2 User Manual* (2015).
- [52] R. Liljestrang, J. McIntyre, G. Blanpied, J. Lynch, L. Ray, W. R. Coker, and G. W. Hoffmann, *Phys. Rev. C* **11**, 1570 (1975).
- [53] M. Beard, E. Uberseder, R. Crowter, and M. Wiescher, *Phys. Rev. C* **90**, 034619 (2014).

- [54] A. Larsen, A. Spyrou, S. Liddick, and M. Guttormsen, *Progress in Particle and Nuclear Physics* **107**, 69 (2019).
- [55] A. Ratkiewicz, J. A. Cizewski, J. E. Escher, G. Potel, J. T. Burke, R. J. Casperson, M. McCleskey, R. A. E. Austin, S. Burcher, R. O. Hughes, B. Manning, S. D. Pain, W. A. Peters, S. Rice, T. J. Ross, N. D. Scielzo, C. Shand, and K. Smith, *Phys. Rev. Lett.* **122**, 052502 (2019).